



Herschel[★]-PACS measurements of nitrogen enrichment in nebulae around Wolf–Rayet stars

D. J. Stock^{1†} and M. J. Barlow²

¹*Department of Physics and Astronomy, University of Western Ontario, Richmond Street, London, ON N6A 3K7, Canada*

²*Department of Physics and Astronomy, University College London, Gower Street, London WC1E 6BT, UK*

Accepted 2014 April 9. Received 2014 April 7; in original form 2014 January 28

ABSTRACT

For three nebulae that have early-WN Wolf–Rayet exciting stars, NGC 6888, WR 8 and Abell 48, we have obtained *Herschel*-PACS line scans of the [N III] 57- μm and [O III] 88- μm lines, along with the 122- and 205- μm lines of [N II]. From the former two lines we have derived $\text{N}^{2+}/\text{O}^{2+}$ abundance ratios, equal to the overall N/O ratio under a wide range of nebular conditions. We find that all of the nebulae observed possess significant nitrogen enrichment, with derived N/O ratios greater than solar. The two nebulae with massive Wolf–Rayet exciting stars, NGC 6888 and WR 8 are found to have N/O ratios that are enhanced by factors of 7–10 relative to the solar N/O ratio, consistent with an origin as material ejected just before the onset of the Wolf–Rayet phase. The other nebula, Abell 48, has recently been reclassified as a member of the rare class of three planetary nebulae that have early-WN central stars and are not of Peimbert type I. We derive a nebular N/O ratio for it that is a factor of 4 enhanced relative to solar and slightly above the range of N/O values that have been measured for the other three members of its [WN] planetary nebula class.

Key words: circumstellar matter – stars: massive – stars: mass-loss – stars: winds, outflows – stars: Wolf–Rayet – ISM: abundances.

1 INTRODUCTION

Core-collapse supernovae from massive stars are known to dominate the production of oxygen and heavier α -particle elements in galaxies but massive stars can make an important contribution to the nitrogen enrichment of the interstellar medium (ISM) during the early evolution of galaxies (Henry, Edmunds & Köppen 2000). This can happen via the ejection of nitrogen-enriched material that has been heavily processed by the CNO cycle during their luminous blue variable (LBV) and ensuing WN Wolf–Rayet (WR) stages.

Observational determinations of the quantities of nitrogen injected into the ISM by WN stars and/or their LBV precursors are limited in number. However, a subset of WR stars is surrounded by nebulae whose expansion ages, morphologies, and occasional abundance determinations (e.g. Esteban et al. 1992; Stock, Barlow & Wesson 2011), show them to consist of nitrogen-rich material that has been recently ejected by the star; these are termed ‘ejecta nebulae’ (Chu 1991; Stock & Barlow 2010).

Amongst the small sample of known, or candidate, WR ejecta nebulae, only a fraction have been probed spectroscopically and

their abundances derived. Such efforts have been hampered by the high degree of extinction along their sight lines in the galactic plane. The usual suite of abundance determination methods (e.g. Torres-Peimbert & Peimbert 1977; Kingsburgh & Barlow 1994; Wesson, Stock & Scicluna 2012) rely on complex empirical relationships to calibrate the densities, temperatures and ionization schemes used to derive reliable abundances. The main stumbling block for these schemes with respect to nebulae around hot, massive stars comes in the lack of optical transitions from some of the ionization states that are expected to dominate the ion populations. For example, nitrogen abundances in nebulae are commonly calculated using the [N II] 6548/6584 Å doublet; however, N^+ is often not the dominant nitrogen ion, so ionization correction factors are employed to attempt to compensate. In addition heavy extinction by interstellar dust towards galactic plane WR stars typically means that the blue end of the optical spectrum is missing, and therefore abundance determinations cannot be easily made (e.g. Stock et al. 2011). At far-infrared (far-IR) wavelengths the effect of dust extinction is essentially removed and the usually dominant ionization stages of oxygen and nitrogen (N^{2+} and O^{2+}) have accessible fine structure lines whose low excitation energies render ionic abundances derived from them insensitive to the adopted nebular electron temperature.

Using the PACS instrument (Poglitsch et al. 2010) on the *Herschel Space Observatory* (Pilbratt et al. 2010), we have obtained spectral data cubes of various fine structure lines in the PACS wavelength range. For each source the [N III] and [O III] lines at 57 and 88 μm

[★]*Herschel* is an ESA space observatory with science instruments provided by European-led Principal Investigator consortia and with important participation from NASA.

[†]E-mail: dstock4@uwo.ca

have been mapped, along with the [N II] lines at 122 and 205 μm , which we will employ to test assumptions about (a) density and (b) the ionization structure.

Our *Herschel* programme (OT2_dstock_3) covered two WR ejecta nebulae (around WR 8 and WR 136, the latter's nebula better known as NGC 6888) along with the PN A66 48 (henceforth Abell 48). At the time of its PACS observations in 2012, Abell 48 was thought to have been generated by a massive WR star but two recent studies have shown it to be a classical PN, albeit one with a rare WN-type central star (Frew et al. 2013; Todt et al. 2013).

2 DATA

2.1 Target selection

Our target sample was drawn from the WR ejecta nebula catalogue of Stock & Barlow (2010). The selection criterion was that the exciting WR star should have a spectral type of WN7 or earlier, or WC7 or earlier, in order that N^{2+} and O^{2+} would be the dominant ion stages of N and O, respectively (this is unlikely to be the case for later type, lower excitation WR central stars).

The ejecta nebula around WR 8 has been observed spectroscopically in the optical (Stock et al. 2011) but due to heavy reddening nebular temperature diagnostics were not available and so no reliable abundances could be derived. However the lower limits quoted by Stock et al. (2011) suggest that the nebula around WR 8 is heavily enriched in nitrogen. The spectral type of WR 8 (WC4/WN7) indicates that it is a transition star, believed to be changing from its nitrogen rich phase (WN) to its carbon rich phase (WC) (Crowther, Smith & Willis 1995). As such the total amount of nitrogen in the nebula should be close to the total amount of nitrogen that will ever be ejected by this star.

The second target, NGC 6888, is one of the best known WR nebulae, having been studied in great detail by many authors [most recently by Fernández-Martín et al. (2012) who present a thorough review]. It is thought to be the result of a major outflow of material whilst the parent star (WR 136; HD 192163; spectral type WN6h) was passing through a red giant phase (Marston 1995).

The third target, the nebula PN Abell 48, has been found to possess an early-WN type central star (Wachter et al. 2010). More recent work (Frew et al. 2013; Todt et al. 2013) has shown that this object is actually much more likely to be a rare type of planetary nebula (PN), with a nitrogen rich low-mass central star (of type [WN]) which mimics the spectral appearance of a more massive WN star. The exact subtype of the central star has been debated, with the Todt et al. (2013) study estimating it to be [WN 5] while Frew et al. (2013) estimated it to be [WN 4–5]. The arguments presented by Frew et al. (2013) to show that the central star is of low mass are twofold. First, if it were a massive star it would be at a very large distance and the mass of the expelled material would be around $50 M_{\odot}$, which is above the initial mass range for massive stars which are thought to become mid-WN subtypes (Crowther 2007). Secondly, the increased distance would place the system behind the galactic bulge and therefore change the expected extinction dramatically, which is not confirmed by their spectra.

2.2 Observations

Herschel/PACS spectra of four fine structure lines between ~ 55 and $\sim 205 \mu\text{m}$ were obtained in line scan mode for each of the objects discussed in the previous section. The PACS spectrometer is an integral field unit (IFU) consisting of a 5×5 array of 9.4 arcsec \times

9.4 arcsec spectral pixels (spaxels). Details of the observations are presented in Table 1, with general information in Table 1(a) and line scan details, including exposure times, in Table 1(b). Fig. 1 shows the spectrometer IFU footprint superimposed on SuperCOSMOS $\text{H}\alpha$ images of the targets.

The PACS spectrometer chopping nodding observation mode was employed for the smallest nebula (Abell 48), while for the larger nebulae the chop throw was not sufficient to find a ‘sky’ field. For WR 8 and NGC 6888 we therefore used the pointed line scan mode, using specific sky fields far from the nebulae. In both types of observation the ‘sky’ fields were used to cancel the emission from the telescope and instruments.

For Abell 48 and WR 8, one on-source field was observed for each object. In fact Abell 48 nearly fills the entire PACS IFU spectrometer field of view, while for the nebula around WR 8 we selected the brightest $\text{H}\alpha$ patch of nebulosity. The large angular size of NGC 6888 allowed us to observe two fields, one at the rim and one near the centre.

Each line scan observation resulted in a spectral cube containing two spatial dimensions with five spaxels along each axis and a wavelength axis encompassing the spectral line and a section of continuum on either side. The spectral resolution of the PACS instrument varies with wavelength and grating order. For [N III] $57 \mu\text{m}$, $R \sim 2700$, while for the [N II] line at $122 \mu\text{m}$ the resolving power was 1100.¹ The wavelength ranges and resolving powers are given for each observation in Table 1(b).

2.3 Data reduction and analysis

Each of the observations was reduced using the standard PACS spectroscopy reduction pipeline within HIPE (v11.0.1; Ott 2010).

The analysis process for the data was relatively simple. Initially, the alignments for each of the different data cubes were checked for each object, i.e. whether the observations of each line covered precisely the same area. It was found that in all cases the deviations were less than 1 arcsec due to slight rotation of the telescope between observations, relative to the field. In order to minimize the effect of the slightly mismatched apertures on the later results, the integrated spectra were calculated using in inner 3×3 array of pixels rather than the whole 5×5 array.

Subsequently, lines in the four spectral data cubes for each observation were measured identically. Each co-added spectrum was fitted with a straight line plus a Gaussian, representing the continuum and line emission, respectively (see Figs 2–5 for an example). The continuum was initially fitted to ‘windows’ of 10 or so pixels on either side of the line to gain a rough estimate of the continuum properties, which were then used as initial conditions for the fit to the continuum and line. For the two instances of [N II] $205\text{-}\mu\text{m}$ line detections a slightly different fitting routine was used because the increased noise in this region rendered the method unreliable. Instead a Gaussian was fitted to the data assuming a continuum, which was set to be constant at the level of the base of the detected line.

A further exception was made for the fit to the weak [N II] $122\text{-}\mu\text{m}$ line from the inner region of NGC 6888. For this spectrum (see Fig. 4) there is clear curvature to the continuum and so the straight

¹ PACS Observer's Manual: http://herschel.esac.esa.int/Docs/PACS/pdf/pacs_om.pdf

Table 1. Log of observations.

Object	RA ^a	Dec. ^b	Chop throw	(a) General characteristics			
				ObsID	Date and time ^c	Lines	Total observing time (s) ^d
WR 8	07 44 50.83	−31 55 15.8	–	1342245246	2012-05-02 10:35:04	[O III] 88 μm, [N II] 205 μm	4646
WR 8 sky	07 44 17.68	−31 52 10.6	–	1342245246	2012-05-02 10:35:04	[O III] 88 μm, [N II] 205 μm	
WR 8	07 44 50.83	−31 55 15.8	–	1342245247	2012-05-02 11:54:37	[N III] 57 μm, [N II] 122 μm	1577
WR 8 sky	07 44 17.68	−31 52 10.6	–	1342245247	2012-05-02 11:54:37	[N III] 57 μm, [N II] 122 μm	
A 48	18 42 46.92	−3 13 17.2	1 arcmin	1342253738	2012-10-21 03:04:59	[N III] 57 μm, [N II] 122, 205 μm	2371
A 48	18 42 46.92	−3 13 17.2	1 arcmin	1342253739	2012-10-21 03:46:43	[O III] 88 μm	814
NGC 6888 (rim)	20 12 39.02	38 26 55.1	–	1342256477	2012-12-06 13:36:56	[O III] 88 μm, [N II] 205 μm	2319
NGC 6888 sky	20 11 34.89	38 25 19.9	–	1342256477	2012-12-06 13:36:56	[O III] 88 μm, [N II] 205 μm	
NGC 6888 (rim)	20 12 39.02	38 26 55.1	–	1342256478	2012-12-06 14:17:45	[N III] 57 μm, [N II] 122 μm	1570
NGC 6888 sky	20 11 34.89	38 25 19.9	–	1342256478	2012-12-06 14:17:45	[N III] 57 μm, [N II] 122 μm	
NGC 6888 (inner)	20 11 56.02	38 21 40.1	–	1342256927	2012-12-09 15:51:16	[O III] 88 μm, [N II] 205 μm	1574
NGC 6888 sky	20 11 34.89	38 25 19.9	–	1342256927	2012-12-09 15:51:16	[O III] 88 μm, [N II] 205 μm	
NGC 6888 (inner)	20 11 56.02	38 21 40.1	–	1342256928	2012-12-09 16:19:46	[N III] 57 μm, [N II] 122 μm	2323
NGC 6888 sky	20 11 34.89	38 25 19.9	–	1342256928	2012-12-09 16:19:46	[N III] 57 μm, [N II] 122 μm	

(b) Exposure times and observation characteristics						
Object	Line	Wavelength range (μm)	Resolving power	Repetitions	Exposure time (s)	
WR 8	[N III] 57 μm	56.95–57.72	≈2800	3	225	
WR 8	[O III] 88 μm	87.77–88.98	≈2400	2	300	
WR 8	[N II] 122 μm	119.98–123.77	≈1100	3	225	
WR 8	[N II] 205 μm	204.11–206.19	≈1700	8	1200	
Abell 48	[N III] 57 μm	57.05–57.64	≈2800	2	384	
Abell 48	[O III] 88 μm	87.92–88.81	≈2400	2	368	
Abell 48	[N II] 122 μm	120.57–123.18	≈1100	2	344	
Abell 48	[N II] 205 μm	204.58–206.04	≈1700	2	344	
NGC 6888 (rim)	[N III] 57 μm	56.95–57.73	≈2800	3	225	
NGC 6888 (rim)	[O III] 88 μm	87.77–88.98	≈2400	2	150	
NGC 6888 (rim)	[N II] 122 μm	119.98–123.77	≈1100	3	225	
NGC 6888 (rim)	[N II] 205 μm	204.16–206.24	≈1700	8	600	
NGC 6888 (inner)	[N III] 57 μm	56.95–57.73	≈2800	3	225	
NGC 6888 (inner)	[O III] 88 μm	87.77–88.98	≈2400	2	150	
NGC 6888 (inner)	[N II] 122 μm	119.98–123.77	≈1100	3	225	
NGC 6888 (inner)	[N II] 205 μm	204.16–206.24	≈1700	8	600	

^aHours, minutes and seconds. ^bDegrees, arcminutes and arcseconds. ^cUT. ^dFor WR 8 and NGC 6888 the sky positions are included in the total OB execution time.

line continuum fit was modified to a second-order polynomial for this source.

An upper limit to the [N II] 122-μm flux for WR 8 was found by initially fitting a second-order polynomial continuum to the observation. Subsequently a Gaussian with the same width as that found for A48 was added and the flux tuned such that the line could just be clearly discerned against the noise – this was adopted as the 3σ upper limit to the line flux.

In order to calculate the signal-to-noise ratio (SNR), we measured the root mean square (rms) noise of the continuum measurement by subtracting the fitted continuum from the data and calculating the rms within the spectral windows previously mentioned. The SNR

of each line was estimated by comparing the integrated line flux to the rms noise taking into account the width of the Gaussian and wavelength spacing of the spectral points.

3 RESULTS

In Table 2 we list integrated line fluxes and some derived quantities for the central 3×3 group of spaxels for the lines of [N III] 57 μm, [O III] 88 μm and [N II] 122, 205 μm. Figures with the line fits to the integrated spectra are shown for WR 8 in Fig. 2, the outer field of NGC 6888 in Fig. 3, the inner field of NGC 6888 in Fig. 4 and for Abell 48 in Fig. 5.

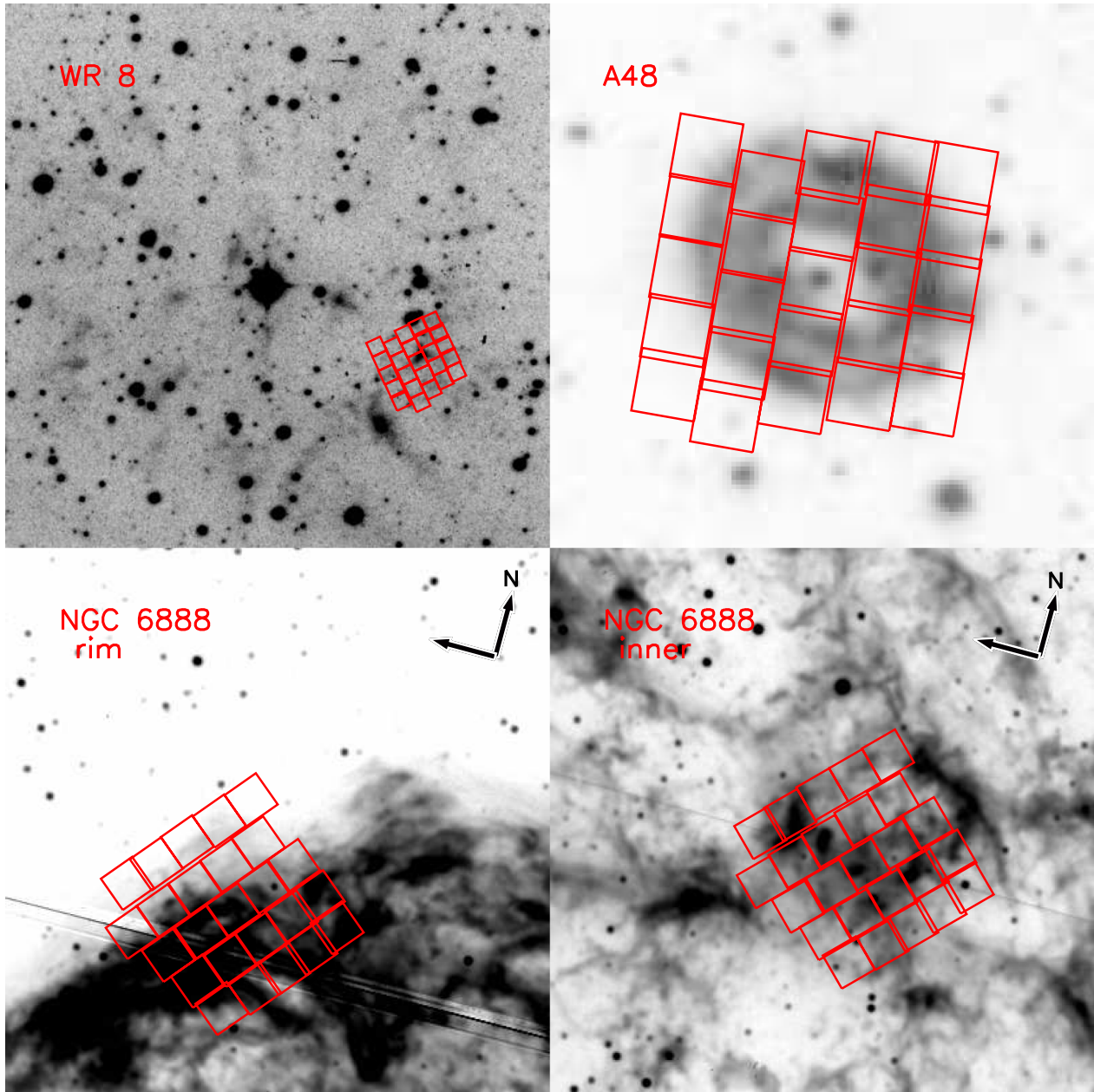


Figure 1. *Herschel* PACS spectrometer fields of view for observed sources. The array of red boxes represents the footprint of the 5×5 array of 9.4 arcsec square pixels. North is up and east is to the left except for the NGC 6888 field where its direction is indicated. Background images are Supercosmos $H\alpha$ Survey imagery for WR 8 and Abell 48 (Parker et al. 2005) and INT photometric $H\alpha$ survey (IPHAS) images for NGC 6888 (Drew et al. 2005).

3.1 Nebular ionization balance and electron densities

As discussed by Liu et al. (2001), for a wide range of nebular excitation classes measured N^{2+}/O^{2+} ratios are expected to be close to the overall nebular N/O ratios, due to the similar ionization potentials of the first and second ion stages of nitrogen and oxygen. However, the $[N\text{ III}]$ 57- μm and $[O\text{ III}]$ 88- μm lines have different critical densities, so nebular electron density estimates are needed when using these lines to evaluate nebular N^{2+}/O^{2+} ratios.

The $[N\text{ II}]$ 122-, 205- μm emission lines were observed with the intention of measuring their relative fluxes, since their flux ratio is an electron density diagnostic. However, the weaker of the two lines, at 205 μm , falls in a poorly calibrated and noisy wavelength region of the PACS spectrometer's wavelength coverage and only two

detections of this line having a SNR greater than 3 were obtained. The 122- μm line was detected, quite strongly in some cases, in all of the nebular spectra except for that of WR 8.

At the low-density limit (e.g. $\sim 1\text{ cm}^{-3}$) the flux ratio of the $[N\text{ II}]$ 122/205- μm lines is predicted to be 0.74, and the ratio approaches its high-density limit ratio of ~ 10 for electron densities above 2000 cm^{-3} . As can be seen from Table 2, for the two cases where detections of $[N\text{ II}]$ 205 μm were made, the 122/205 flux ratio is found to be 25 and 56. Since the optically determined electron densities for all of the nebulae are below 1000 cm^{-3} , we attribute this discrepancy to the problems in calibrating PACS spectra longwards of 190 μm due to the leak of shorter wavelength radiation that affects this spectral region (Poglitsch et al. 2010). Instead, we have adopted electron densities measured at optical wavelengths

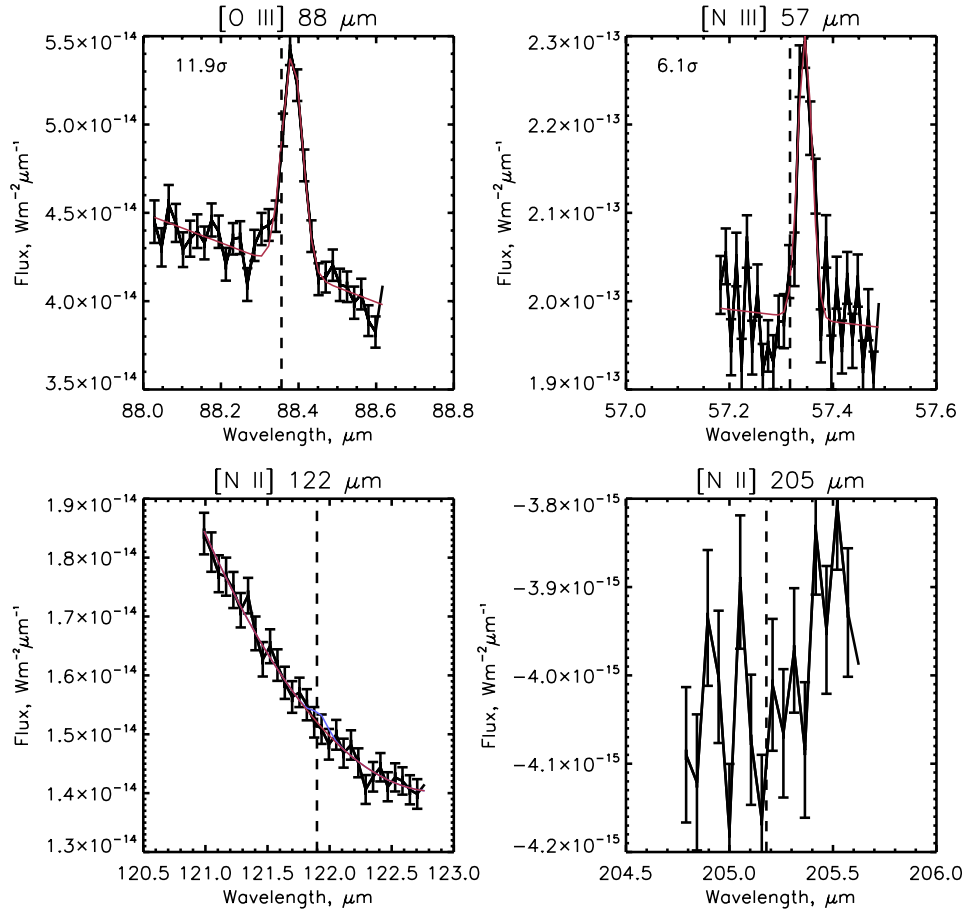


Figure 2. Integrated spectra (black) and line fits (red) to PACS line scans for the nebula around WR 8, clockwise from top left: [O III] 88 μm , [N III] 57 μm , [N II] 205 μm and [N II] 122 μm . The derived line SNR are indicated for each fit. For the [N II] 122- μm line we include a Gaussian with the upper flux limit (blue).

(Table 2). A number of different regions of NGC 6888 were studied by Fernández-Martín et al. (2012) and values of n_e of 100 and 200 cm^{-3} were found for fields close to those we observed with PACS. For WR 8, Stock et al. (2011) found a nebular electron density of $n_e \sim 50 \text{ cm}^{-3}$, while for Abell 48 Frew et al. (2013) found an electron density of 700 cm^{-3} – consistent with our strong 57- and 88- μm line detections.

We have used our detections of the [N II] 122- μm and [N III] 57- μm lines to calculate the N^{2+}/N^+ abundance ratio for each of the three nebulae for which the [N II] 122- μm line was detected. The EQUIB code, developed at UCL by Howarth and Adams, was used to solve the statistical equilibrium equations for multilevel atomic models of N^{2+} and N^+ , giving level populations and line emissivities for the appropriate physical conditions. The atomic data used by EQUIB are from the CHIANTI atomic data base (Landi et al. 2006). Detailed references for the collision strengths and transition probabilities can be found in Table 3.

From the atomic data, the relationship between the line intensities and the ionic abundances was found. At the low-density limit for both lines this resolves to $\text{N}^{2+}/\text{N}^+ \simeq 0.22 \times (I_{57} / I_{122})$, where I_{57} , I_{122} are the fluxes of the 122- and 57- μm lines, respectively. At the high-density limit for both lines the factor of 0.22 becomes 0.08. For each nebula we calculated the appropriate factors using the literature electron densities listed in Table 2. Conservative uncertainties of 50 per cent have been assumed for the electron densities and these are included in the final uncertainties quoted in Table 2. For two of the

three observed fields for which the [N II] 122- μm line was detected, the N^{2+}/N^+ ratio is greater than unity, indicating that N^{2+} is the dominant ionization state of nitrogen. Given the similarity of their ionization potentials, we conclude that O^{2+} is also the dominant ionization state for oxygen in the observed fields.

3.2 N/O ratios and nitrogen enrichment

For each nebula, the conversion factor to be divided into the measured [N III] to [O III] line intensity ratio to obtain the $\text{N}^{2+}/\text{O}^{2+}$ ratio was calculated using EQUIB. These factors ranged from around 1.5 at the lowest electron densities considered (50 cm^{-3}) to 2.3 at the highest density (700 cm^{-3}). The uncertainties quoted in Table 2 include a 50 per cent uncertainty in the electron densities adopted from the literature. From a comparison of the nebular N/O ratios found in Table 2 with the solar and Galactic H II region N/O ratios of 0.12–0.14 (Asplund et al. 2009; Stock et al. 2011), it can be seen that the N/O ratios of the two massive WR nebulae are enriched by factors of 7 to 10 relative to the solar ratio, while the N/O ratio of the [WN] PN Abell 48 is enhanced by a factor of 4.

Our measured N/O ratios are consistent with previous measurements, which, due to the absence of lines of [N III] in the optical region, had been based on the ratio of the ion stages N^+ and O^+ . To provide context to the abundances calculated for our sample, we have included Table 4, which shows the results of prior studies, sorted by the spectral type of the host star.

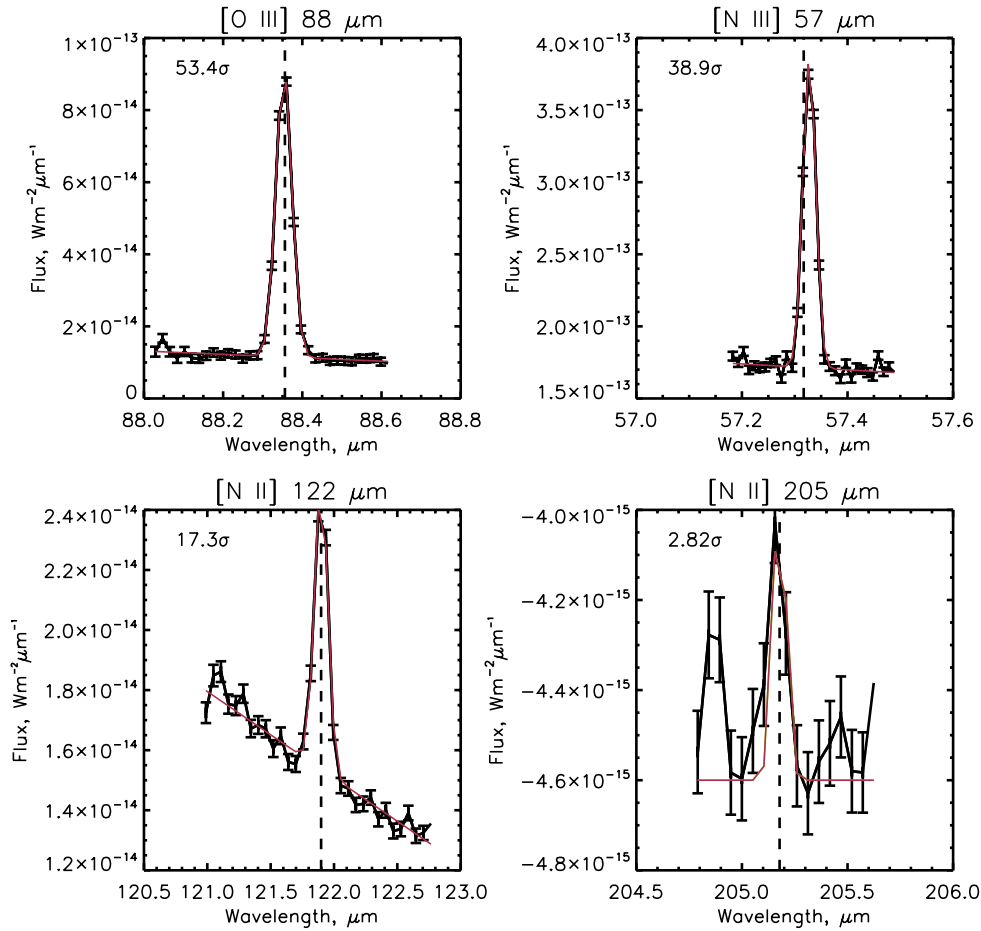


Figure 3. Integrated spectra (black) and line fits (red) to PACS line scans for NGC 6888 (outer), clockwise from top left: [O III] 88 μm , [N III] 57 μm , [N II] 205 μm , [N II] 122 μm . Line SNR are indicated for each fit.

3.2.1 WR 8

From optical spectroscopy of the nebula around WR 8, Stock et al. (2011) found N/O ratios in the range $0.5 < \text{N/O} < 1.25$, consistent with our measurement here of 0.92 ± 0.17 . Our non-detection of the far-IR [N II] lines is likely due to a combination of a low fractional N^+ abundance and the intrinsic faintness of the source. The nebula around WR 8 is likely to be composed of stellar ejecta processed by the CNO cycle. The enhanced nitrogen abundance is characteristic of material ejected during the red supergiant phase (see e.g. NGC 6888). The WN/WC type of the central star indicates that it is more evolved than the other known WR ejecta nebulae (Crowther et al. 1995), consistent with its fainter nebula.

In comparison with the abundances found for other WR nebulae presented in Table 4, the N/O ratio we find for the nebula around WR 8 is actually rather modest. This, combined with the advanced evolutionary state of the system, suggests that there is a substantial component of swept-up ISM in the nebula.

3.2.2 NGC 6888

Optical N^+/O^+ ratios were measured by Fernández-Martín et al. (2012) for NGC 6888, who found values of 0.74–1.20 near to the ‘rim’ region for which we found an $\text{N}^{2+}/\text{O}^{2+}$ ratio of 0.93 ± 0.08 , and an N^+/O^+ ratio of 0.18–0.48 for a central region close to where we found $\text{N}^{2+}/\text{O}^{2+} = 1.25 \pm 0.07$. The earlier optical spectroscopic

study of Esteban & Vilchez (1992) found an N^+/O^+ ratio of ~ 2 for the blue- and redshifted shell components of the nebula, while an ambient gas velocity component showed a more solar-like N^+/O^+ ratio. A more recent study by Mesa-Delgado et al. (2014) found a much higher value of $\text{N/O} = 1.65$ for a field closer to the exciting star than our inner field, possibly representing more recent stellar ejecta with respect to that measured at greater distances.

Clear differences are evident between the two NGC 6888 fields. The rim field has stronger [N II] lines and an N^{2+}/N^+ ratio of 0.7, consistent with representing material far from the exciting star. In contrast, the central field shows much weaker [N II] lines relative to the [N III] 57- μm line.

The N/O ratios found for NGC 6888 are again moderate compared to the extreme examples in Table 4. The lower abundances in the rim of NGC 6888 suggest that the rim regions include a large swept-up ISM component. However, Fernández-Martín et al. (2012) found the opposite trend in that their highest N/O ratio was found for a bright section of the rim of NGC 6888. This could be an ionization effect though as the N/O ratio quoted by Fernández-Martín et al. (2012) is N^+/O^+ , and these ionization stages are unlikely to be dominant as discussed earlier.

3.2.3 Abell 48

Abell 48 has been shown to be a PN with an early-WN central star (Frew et al. 2013; Todt et al. 2013). The former authors found an

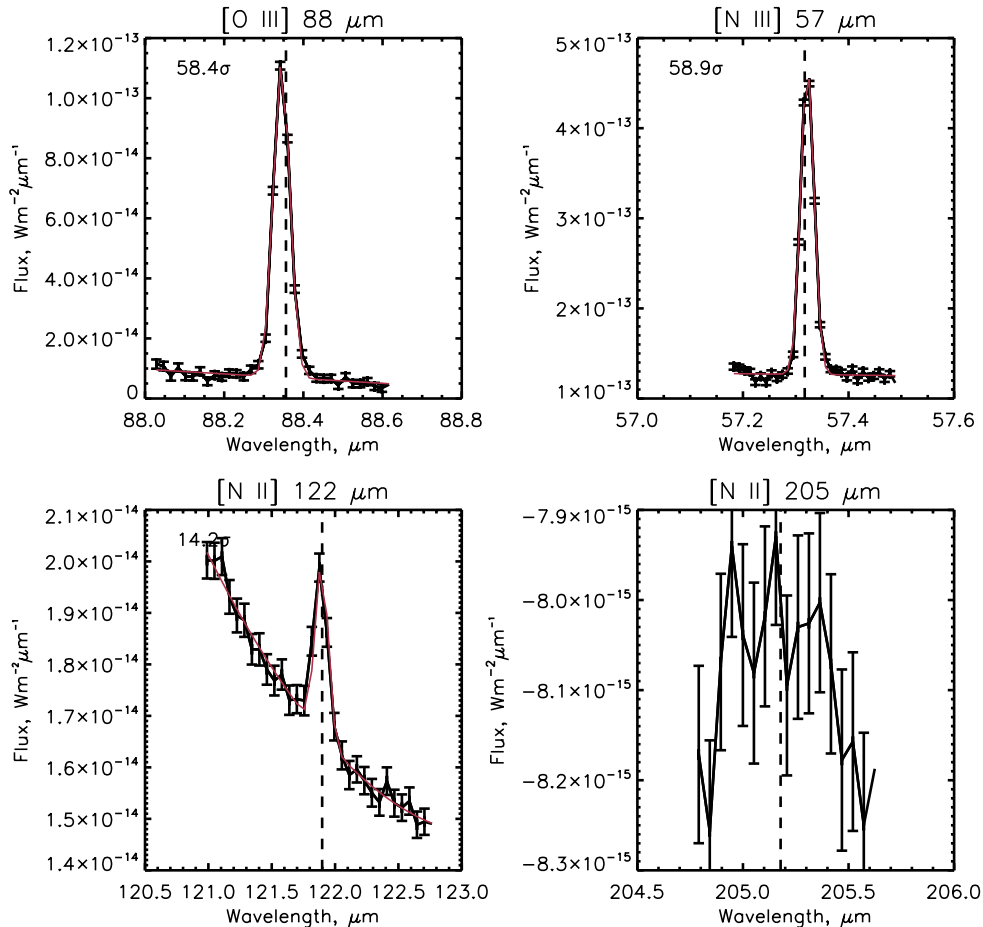


Figure 4. Integrated spectra (black) and line fits (red) to PACS line scans for NGC 6888 (inner), clockwise from top left: [O III] 88 μm , [N III] 57 μm , [N II] 205 μm , [N II] 122 μm . Line SNR are indicated for each fit.

N^+/O^+ ratio of 0.25 ± 0.10 for Abell 48, while the latter authors found an N^+/O^+ ratio of 0.12. In addition, an N/O ratio of 0.27 has been quoted by Danehkar et al. (2014). Our N^{2+} - and O^{2+} -based measurement of $\text{N}/\text{O} = 0.49 \pm 0.06$ does not agree with these measurements by almost a factor of two. However, the detailed photoionization models of Danehkar et al. (2014) predict N^{2+} and O^{2+} abundances which, when combined yield an $\text{N}^{2+}/\text{O}^{2+}$ ratio of 0.52, which matches that observed.

Abell 48 has a large N^{2+}/N^+ ratio of 7.3 (Table 2). The nebular spectra of Todt et al. (2013) and Frew et al. (2013) showed no He II or $[\text{Ar IV}]$ line emission, indicating a lack of stellar photons with energies in excess of 54.4 eV, so we conclude that N^{2+} and O^{2+} are the dominant ion stages of nitrogen and oxygen and that our $\text{N}^{2+}/\text{O}^{2+}$ -based N/O ratio for Abell 48 should therefore be accurate.

The other three objects in the rare class of PNe having WN central stars have been found to have N/O ratios ranging from 0.28 to 0.4 (LMC-N66: Tsamis et al. 2003, $\text{N}/\text{O} = 0.4$; PB 8: García-Rojas, Peña & Peimbert 2009, $\text{N}/\text{O} = 0.28$; IC 4663: Miszalski et al. 2012, $\text{N}/\text{O} = 0.36$). Each of these studies had access not only to the optical lines of [N II] but also to the ultraviolet N III] and N IV] lines. Our measurement of $\text{N}/\text{O} = 0.49 \pm 0.06$ for Abell 48 falls slightly above the N/O ratios found for the Galactic members of this class (IC 4663 and PB 8).

3.3 Predicted stellar yields and swept-up material

Toalá & Arthur (2011) computed models for the ejecta from massive stars and calculated the degree of nitrogen enrichment that would be expected in the nebulae as a function of time. They found that the N/O values seen in NGC 6888 and S 308, the two best known WR bubbles, are characteristics of a $\sim 3 \times 10^5$ yr WR period in the life of 40–60 M_{\odot} stars (see Toalá & Arthur 2011, fig. 16). They are also consistent with the N/O ratios that we find here for NGC 6888 and WR 8.

However, it should be noted that the results of Toalá & Arthur (2011) do not include the effect of the nebulae sweeping up ISM material and hence diluting the detected nebular abundances. From Table 4 it is clear that the highest N/O ratios detected for classical WR nebulae are for M 1-67, one of the most compact of the class with a radius of around 1.2 pc (Fernández-Martín et al. 2013). If we assume that this is a reasonable benchmark for the abundances of a WR nebula containing very little swept-up material, it is clear that the other nebulae listed in Table 4 must suffer from considerable dilution of their natal abundances. For consistency then, models such as those of Toalá & Arthur (2011) should find much higher N/O ratios than observed, such that they would reproduce the observed abundances after ISM dilution was taken into account.

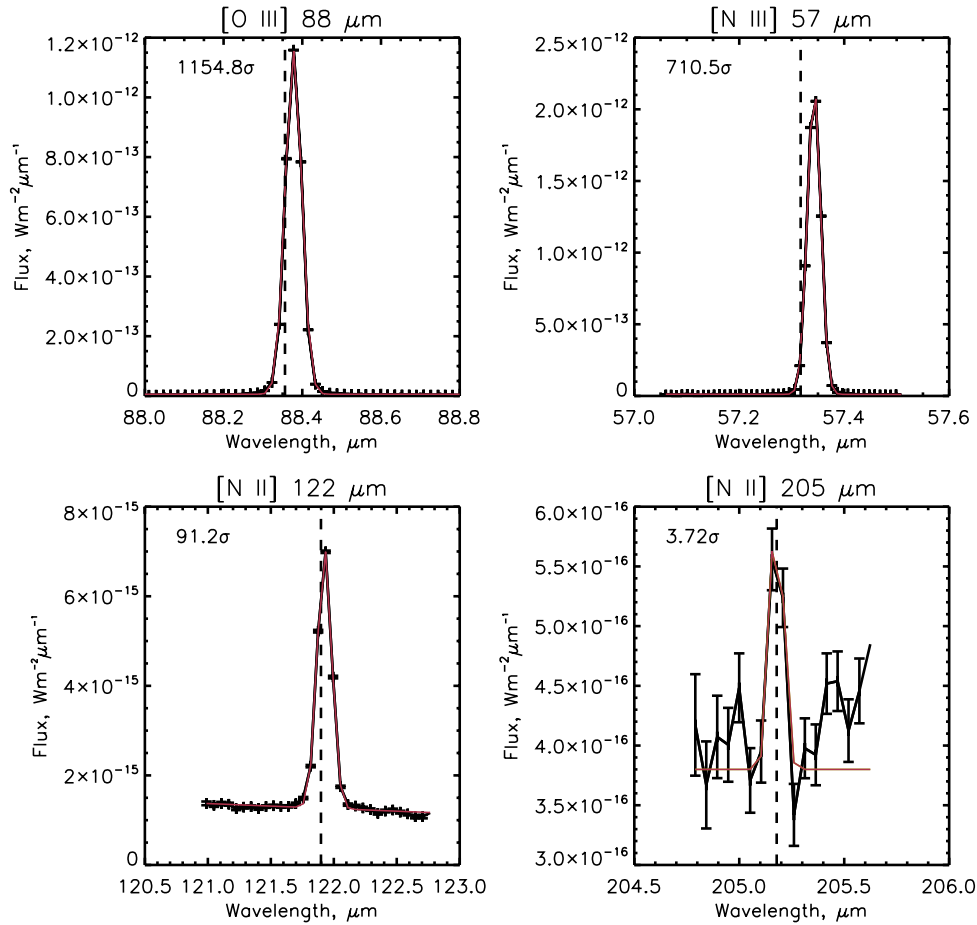


Figure 5. Integrated spectra (black) and line fits (red) to PACS line scans for Abell 48, clockwise from top left: [O III] 88 μm , [N III] 57 μm , [N II] 205 μm , [N II] 122 μm . Line SNR are indicated for each fit.

Table 2. Integrated nebular properties.

Object	Fluxes ^a				Abundances		
	[O III] 88 μm	[N III] 57 μm	[N II] 122 μm	[N II] 205 μm	N^{2+}/N^+	$\text{N}^{2+}/\text{O}^{2+} = \text{N}/\text{O}$	$n_e(\text{cm}^{-3})$
WR 8	8.08 ± 0.68	11.11 ± 1.81	<0.30	–	>7.78	0.92 ± 0.17	50^b
NGC 6888 (rim)	40.34 ± 0.76	65.88 ± 1.70	12.55 ± 0.72	0.50 ± 0.18	0.68 ± 0.07	0.93 ± 0.08	200^c
NGC 6888 (inner)	54.62 ± 0.94	108.70 ± 1.85	4.28 ± 0.30	–	4.06 ± 0.39	1.25 ± 0.07	100^c
A 48	602.92 ± 0.52	680.93 ± 0.96	8.41 ± 0.09	0.18 ± 0.05	7.29 ± 0.81	0.49 ± 0.06	700^d

^a $\times 10^{-13} \text{ W m}^{-2}$. ^bStock et al. (2011). ^cFernández-Martín et al. (2012). ^dFrew et al. (2013).

Table 3. Sources of atomic data.

Ion	References
N^+	A Values: Bell, Hibbert & Stafford (1995), Storey & Zeippen (2000); Collision strengths: Stafford et al. (1994b)
N^{2+}	A Values: Nussbaumer & Storey (1979); Collision strengths: Stafford, Bell & Hibbert (1994a)
O^{2+}	A Values: Storey & Zeippen (2000); Tachiev & Fischer (2001); Collision strengths: Lennon & Burke (1994)

4 CONCLUSIONS

The degree of nitrogen enrichment in a selection of nebulae around WR stars has been measured using *Herschel*/PACS observations of their far-IR fine structure lines. Abundance studies are usually performed using optical spectra, which has the drawback of not including any lines of N^{2+} , which is often the dominant ionization stage for nitrogen. This effect is usually compensated for using ionization correction factor schemes to calculate the N^{2+} abundance. The far-IR observations used in this paper include the 57- μm line of N^{2+} , which should result in nitrogen abundances that are less susceptible to systematic errors. In addition, abundances obtained for N^+ , N^{2+} and O^{2+} from their far-IR lines have little or no sensitivity to the nebular electron temperature, due to their low excitation energies.

Table 4. Enrichment of nitrogen in nebulae around massive WR stars.

Nebula	Star	Spectral type	Nebular N/O	Reference
S 308	WR 6	WN4	0.54	Kwitter (1984)
S 308	WR 6	WN4	1.65	Esteban et al. (1992)
NGC 2359	WR 7	WN4	0.11	Esteban et al. (1992)
NGC 3199	WR 18	WN4	0.20	Kwitter (1984)
NGC 3199	WR 18	WN4	0.12	Stock et al. (2011)
RCW 104	WR 75	WN6	0.74	Esteban et al. (1992)
NGC 6888	WR 136	WN6h	0.50	Esteban & Vilchez (1992)
NGC 6888	WR 136	WN6h	0.50	Moore, Hester & Scowen (2000)
NGC 6888 (rim ^a)	WR 136	WN6h	1.20	Fernández-Martín et al. (2012)
NGC 6888 (inner ^b)	WR 136	WN6h	0.97	Fernández-Martín et al. (2012)
NGC 6888 (inner)	WR 136	WN6h	1.65	Mesa-Delgado et al. (2014)
NGC 6888 (rim)	WR 136	WN6h	0.93	This work
NGC 6888 (inner)	WR 136	WN6h	1.25	This work
anon	WR 8	WC4/WN7	>0.4	Stock et al. (2011)
anon	WR 8	WC4/WN7	0.92	This work
anon	WR 16	WN8h	high	Marston et al. (1999)
anon	WR 16	WN8h	>0.8	Stock et al. (2011)
RCW 58	WR 40	WN8h	0.38	Kwitter (1984)
RCW 58	WR 40	WN8h	>1.25	Stock et al. (2011)
M 1-67	WR 124	WN8h	2.95	Esteban et al. (1991)
M 1-67	WR 124	WN8h	2.81	Fernández-Martín et al. (2013)

^aRegion X1, ^bRegion MB1.

The N/O ratios of 0.9–1.3 found for the massive WR-star nebulae WR 8 and NGC 6888 are consistent with both nebulae representing material ejected during the pre-WR evolution of the stars. For NGC 6888, our measurements overlap those of previous authors who employed ionization correction factors to determine the N/O ratio from optical lines. Our observations confirm that the nebula around WR 8 has a significant component of ejected stellar material – as predicted by the morphological categorization methods of Chu (1991) which were employed by Stock & Barlow (2010) upon discovery of the nebulosity.

The other object observed, Abell 48, is now known to be a rare type of PN with a WN4-type central star and which is not of Peimbert type I. Our far-IR observations yield a nebular N/O ratio of 0.49, which is slightly greater than the ratios found for the two other Galactic members of the rare [WN] class of PNe.

ACKNOWLEDGEMENTS

We thank the anonymous referee for their suggestions which have helped improve and clarify the paper. DJS acknowledges support from an NSERC Discovery Grant and an NSERC Discovery Accelerator Grant. This research has made use of NASA's Astrophysics Data System Bibliographic Services. DJS thanks A. Danehkar for alerting us to a mistake in the unit conversions in the first version of this paper.

REFERENCES

Asplund M., Grevesse N., Sauval A. J., Scott P., 2009, *ARA&A*, 47, 481
 Bell K. L., Hibbert A., Stafford R. P., 1995, *Phys. Scr.*, 52, 240
 Chu Y. H., 1991, in van der Hucht K. A., Hidayat B., eds, *Proc. IAU Symp.* 143, *Wolf-Rayet Stars and Interrelations with Other Massive Stars in Galaxies*. Kluwer, Dordrecht, p. 349
 Crowther P. A., 2007, *ARA&A*, 45, 177
 Crowther P. A., Smith L. J., Willis A. J., 1995, *A&A*, 304, 269

Danehar A., Todt H., Ercolano B., Kniazev A. Y., 2014, *MNRAS*, 439, 3605
 Drew J. E. et al., 2005, *MNRAS*, 362, 753
 Esteban C., Vilchez J. M., 1992, *ApJ*, 390, 536
 Esteban C., Vilchez J. M., Manchado A., Smith L. J., 1991, *A&A*, 244, 205
 Esteban C., Vilchez J. M., Smith L. J., Clegg R. E. S., 1992, *A&A*, 259, 629
 Fernández-Martín A., Martín-Gordón D., Vilchez J. M., Pérez Montero E., Riera A., Sánchez S. F., 2012, *A&A*, 541, A119
 Fernández-Martín A., Vilchez J. M., Pérez-Montero E., Candian A., Sánchez S. F., Martín-Gordón D., Riera A., 2013, *A&A*, 554, A104
 Frew D. J. et al., 2013, *MNRAS*, 440, 1345
 García-Rojas J., Peña M., Peimbert A., 2009, *A&A*, 496, 139
 Henry R. B. C., Edmunds M. G., Köppen J., 2000, *ApJ*, 541, 660
 Kingsburgh R. L., Barlow M. J., 1994, *MNRAS*, 271, 257
 Kwitter K. B., 1984, *ApJ*, 287, 840
 Landi E., Del Zanna G., Young P. R., Dere K. P., Mason H. E., Landini M., 2006, *ApJS*, 162, 261
 Lennon D. J., Burke V. M., 1994, *A&AS*, 103, 273
 Liu X.-W. et al., 2001, *MNRAS*, 323, 343
 Marston A. P., 1995, *AJ*, 109, 1839
 Marston A. P., Welzmilller J., Bransford M. A., Black J. H., Bergman P., 1999, *ApJ*, 518, 769
 Mesa-Delgado A., Esteban C., García-Rojas J., Reyes-Pérez J., Morisset C., Bresolin F., 2014, *ApJ*, 785, 100
 Miszalski B., Crowther P. A., De Marco O., Köppen J., Moffat A. F. J., Acker A., Hillwig T. C., 2012, *MNRAS*, 423, 934
 Moore B. D., Hester J. J., Scowen P. A., 2000, *AJ*, 119, 2991
 Nussbaumer H., Storey P. J., 1979, *A&A*, 71, L5
 Ott S., 2010, in Mizumoto Y., Morita K.-I., Ohishi M., eds, *ASP Conf. Ser. Vol. 434, Astronomical Data Analysis Software and Systems XIX*. Astron. Soc. Pac., San Francisco, p. 139
 Parker Q. A. et al., 2005, *MNRAS*, 362, 689
 Pilbratt G. L. et al., 2010, *A&A*, 518, L1
 Poglitsch A. et al., 2010, *A&A*, 518, L2
 Stafford R. P., Bell K. L., Hibbert A., 1994a, *MNRAS*, 266, 715
 Stafford R. P., Bell K. L., Hibbert A., Wijesundera W. P., 1994b, *MNRAS*, 268, 816
 Stock D. J., Barlow M. J., 2010, *MNRAS*, 409, 1429
 Stock D. J., Barlow M. J., Wesson R., 2011, *MNRAS*, 418, 2532

- Storey P. J., Zeppen C. J., 2000, MNRAS, 312, 813
Tachiev G., Fischer C. F., 2001, Can. J. Phys., 79, 955
Toalá J. A., Arthur S. J., 2011, ApJ, 737, 100
Todt H. et al., 2013, MNRAS, 430, 2302
Torres-Peimbert S., Peimbert M., 1977, Rev. Mex. Astron. Astrophys., 2, 181
Tsamis Y. G., Barlow M. J., Liu X.-W., Danziger I. J., Storey P. J., 2003, MNRAS, 345, 186
Wachter S., Mauerhan J. C., Van Dyk S. D., Hoard D. W., Kafka S., Morris P. W., 2010, AJ, 139, 2330
Wesson R., Stock D. J., Scicluna P., 2012, MNRAS, 422, 3516

This paper has been typeset from a $\text{\TeX}/\text{\LaTeX}$ file prepared by the author.